Chalcogenide Letters Vol. 21, No. 2, February 2024, p. 201 - 215

Structural and spectroscopic correlation in barium-boro-tellurite glass hosts: effects of Dy_2O_3 doping

S. F. Hathot[a,*], B. M. Al Dabbagh[a], H. Aboud[b]
[a]*Applied Science Dep, University of Technology, Baghdad, Iraq*
[b]*Faculty of science- physics Dep, college of Science, Al-Mustansiriya University, Iraq*

In this study, a series of barium-boro-tellurite glass hosts with varying concentration of Dy_2O_3 doping (0 to 1.25 mol%) were made by melt-quenching method. A study was conducted to investigate how Dy_2O_3 dopants affect the physical and spectroscopic traits of glasses. Raw materials including barium oxide (BaO), tellurium dioxide (TeO_2), boron oxide (B_2O_3), and dysprosium oxide (Dy_2O_3) were used to produce these glasses. XRD patterns of the samples showed a broad hump and absence of long-range periodic lattice arrangements, indicating their amorphous nature. The Raman spectral analyses displayed the various vibration modes where the most intense band caused by BaO vibrations at 300 cm-1 and 450 cm-1 corresponding to the symmetric stretching vibration mode of Te–O–Te intra-chain bridges. The peak at 750 cm-1 was due to TeO_4 and Te-O-Te vibration modes. The value of optical band gap energy was decreased from 3.155 to 2.1894 eV and then increase at higher Dy_2O_3 level (0.75 to 1.25 mol%). At Dy3+ contents between 0.25 to 1.25 mol% seven absorption bands were observed at 390, 424, 452, 750, 797, 895 and 1092 nm due to the electronic transitions in Dy^{3+}. The glass refractive indices were raised from 2.3563 to 2.6584 and then decreased at higher Dy_2O_3 contents which was mainly because of the generation of more bridging oxygen (BO) in the glass matrix. The value of glass electronic polarizability and oxide ions polarizability calculated using Lorentz-Lorenz equation showed a decrease with the rise of Dy_2O_3 contents, which was ascribed to the presence of fewer non-bridging oxygen (NBO). The optical basicity of the proposed glass hosts was calculated using Duffy and Ingram equation which was decreased with the increase of doping contents. In addition, the optical transmission was increased and reflection loss was reduced with increasing Dy^{+3} levels. The value of metallization parameter below 1 proved the true amorphous nature of the prepared samples. All the glasses revealed blue and yellow photoluminescence emission peaks due to 4F9/2→ 6H15/2, and 4F9/2 →6H13/2 transitions in Dy^{3+}, respectively. The proposed glass compositions may be beneficial for the advancement of solid-state lasers.

(Received November 23, 2023; Accepted February 22, 2024)

Keywords: Dy_2O_3 doping, Raman spectra, Structure, Absorption, Emission

1. Introduction

Tellurium glass system made of TeO_2 as a host has been attracting much interest over the past few years because of enhanced chemical and physical characteristics when compared with oxide glasses such silicates. These glasses have large values of thermoelectric constant, infrared transmittance, dielectric constant and refractive index; low phonon energy cut-off and melting point; very high rare-earth ions solubility [1]. Tellurite-based glasses can also be doped with various rare earth elements to achieve improved optical characteristics that result from the electronic transitions in the rare earth ions. When rare earth ions are added to tellurite glass, they can cause changes in the network structure, including the formation of rare earth oxide clusters or the coordination 2 of rare earth ions with oxygen atoms [2, 3]. The spectroscopic attributes of such glasses can be modified via the structural alterations, indicating a strong correlation between these properties that are controlled by the rare earth elements doping. Tellurite glass with rare earth ions

* Corresponding author: as.21.25@grad.uotechnology.edu.iq
https://doi.org/10.15251/CL.2024.212.201

doping is useful for the fiber optics, optical amplifiers, and lasers, among other applications [4]. For example, erbium-doped tellurite glasses were used in the fiber amplifiers for telecommunications and in the infrared lasers. In addition, tellurite glasses doped with neodymium were used in solid-state lasers for medical and industrial applications.

Despite many experimental studies on this glass system a spectroscopic and structural correlation has not been developed yet, which may provide an in-depth knowledge on the customization of various properties of the tellurite glass system. The addition of Dy_2O_3 into the glasses enhances their optical properties, enabling them suitable for the applications in optoelectronics and photonics. [2]. The addition of Dy_2O_3 into glass can also improve the luminescent properties of the material, making it useful in devices that require efficient light transmission. Furthermore, the improved thermal and electrical characteristics of the tellurite glass hosts make them ideal candidate for various components that require an effective heat and electricity transport. In short, Dy_2O_3 as dopant is very promising material for numerous industrial applications [5]. The tellurium atoms in the glass form covalent bonds with oxygen atoms to create the TeO_4 tetrahedra, which are then interconnected through shared oxygen atoms to form a three-dimensional network. The addition of other elements can modify the structure and properties of the glass, for example, by introducing Oxygen molecules without bridges ,which can lead to a decrease in glass stability [6]. Hazlin et al. [6] made some zinc-boro-tellurite glasses with various levels of Dy^{3+} to determine its effect on their physical, structural and optical characteristics. The values of direct and indirect energy band gap of these glasses were found to increase and Urbach energy was decreased with the Dy_2O_3 concentration, indicating the presence of fewer non-bridging oxygen (NBO) atoms in the glass matrix. Halimah [7] studied the zinc-boro-tellurite glasses with Dy_2O_3 as dopants and observed an increase in their optical band gap energies (both indirect and direct) [8] and decrease in the Urbach energy, oxide ions and electronic polarizabilities, as well as optical basicity with the increase of Dy_2O_3 doping level [8]. Repeated studies have concluded that the tellurite glass system doped with Dy^{3+} display enhanced NIR absorption as well as improved visible-NIR emission. The absorption and emission intensities of these glasses increase at higher doping contents of Dy^{3+} and other lanthanides like Er^{3+} and Yb^{3+} [9]. Due to their ability to act as sensitizers, Dy^{3+} can enhance the spectroscopic and structural properties of the glasses when doped with these ions [10]. Overall, the Dy^{3+}-doping into the tellurite glass system became advantageous for developing low-cost and durable materials with enhanced optical properties needed for various applications in optics and photonics [11]. Looking at the benefits of Dy^{3+}-doped tellurite glass system we made six barium-boro-tellurite glass samples at various doping contents of Dy_2O_3 (0 to 1.25 mol%). The role of Dy_2O_3 doping towards the improvement of structures, physical and optical properties of the proposed glasses was analysed. The prepared glass samples were characterized using various analytical tools to establish a correlation between structural and spectroscopic characteristics., which may provide an in-depth knowledge on the customization of various properties of the tellurite glass system. The addition of Dy2O3 into the glasses enhances their optical properties, enabling them suitable for the applications in optoelectronics and photonics. [2]. The addition of Dy_2O_3 into glass can also improve the luminescent properties of the material, making it useful in devices that require efficient light transmission. Furthermore, the improved thermal and electrical characteristics of the tellurite glass hosts make them ideal candidate for various components that require an effective heat and electricity transport. In short, Dy_2O_3 as dopant is very promising material for numerous industrial applications [5]. The tellurium atoms in the glass form covalent bonds with oxygen atoms to create the TeO4 tetrahedra, which are then interconnected through shared oxygen atoms to form a three-dimensional network. The addition of other elements can modify the structure and properties of the glass, for example, by introducing Oxygen molecules without bridges, which can lead to a decrease in glass stability [6]. Hazlin et al. [6] made some zinc-boro-tellurite glasses with various levels of Dy^{3+} to determine its effect on their physical, structural and optical characteristics. The values of direct and indirect energy band gap of these glasses were found to increase and Urbach energy was decreased with the Dy2O3 concentration, indicating the presence of fewer non-bridging oxygen (NBO) atoms in the glass matrix. Halimah [7] studied the zinc-boro-tellurite glasses with Dy_2O_3 as dopants and observed an increase in their optical band gap energies (both indirect and direct) [8] and decrease in the Urbach energy, oxide ions and electronic polarizabilities, as well as optical basicity with the increase of

Dy_2O_3 doping level [8]. Repeated studies have concluded that the tellurite glass system doped with Dy^{3+} display enhanced NIR absorption as well as improved visible-NIR emission. The absorption and emission intensities of these glasses increase at higher doping contents of Dy^{3+} and other lanthanides like Er^{3+} and Yb^{3+} [9]. Due to their ability to act as sensitizers, Dy^{3+} can enhance the spectroscopic and structural properties of the glasses when doped with these ions [10]. Overall, the Dy^{3+}-doping into the tellurite glass system became advantageous for developing low-cost and durable materials with enhanced optical properties needed for various applications in optics and photonics [11]. Looking at the benefits of Dy^{3+}-doped tellurite glass system we made six barium-boro-tellurite glass samples at various doping contents of Dy_2O_3 (0 to 1.25 mol%). The role of Dy_2O_3 doping towards the improvement of structures, physical and optical properties of the proposed glasses was analyzed. The prepared glass samples were characterized using various analytical tools to establish a correlation between structural and spectroscopic characteristics.

2. Experimental procedures

Melt-quench approach was followed to prepare the new glass system. Table 1 shows the ratios of various raw materials, including barium oxide (BaO), tellurium dioxide (TeO_2), boron oxide (B_2O_3), and trivalent dysprosium oxide (Dy_2O_3) together with the sample code. After weighing and mixing the chemical powders, a platinum crucible containing the mix was placed in an electric furnace at 970 °C for 30 minutes to melt it completely. Three hours of annealing at 350 °C were conducted in a separate furnace. For optical measurements, to ensure flat and parallel surfaces, the obtained glasses were shaped and polished. A few glass pieces were powdered for the structural analysis, silicon carbide paper with different grids was used to polish both sides of the fabricated samples to a thickness of about 3 mm. Using a UV–VIS spectrophotometer (Shimadzu, model UV-1650PC) optical absorption measurement was carried out in the wavelength range of 220 to 1100 nm. To produce fine powder of the prepared samples, a plunger was used to crush them flowed by grinding using a mortar-pestle. XRD and Raman Spectral measurements were performed to analyze the structures of the samples.

Table 1. Codes of the prepared samples and compositions.

Sample code	*Concentrations (mol%)*			
	B_2O_3	BaO	TeO_2	Dy_2O_3
BBTD0%	50	25	25	0.00
BBTD0.25%	49.75	25	23	0.25
BBTD0.5%	49.5	25	25	0.50
BBTD0.75%	49.25	25	25	0.75
BBTD1%	49	25	25	1.00
BBTD1.25%	48.25	25	25	1.25

3. Results and discussion

3.1. Structural analyses of glass

Figure 1 shows XRD patterns of the fabricated samples. The appearance of a broad hump indicated their amorphous character without any long-range periodic lattice arrangements because disordered samples are lack of sharp lines and peaks. Thus, the obtained samples were glasses because the atoms do not have any uniform spacing thereby unable to produce sharp diffraction peaks in the XRD profiles [12]

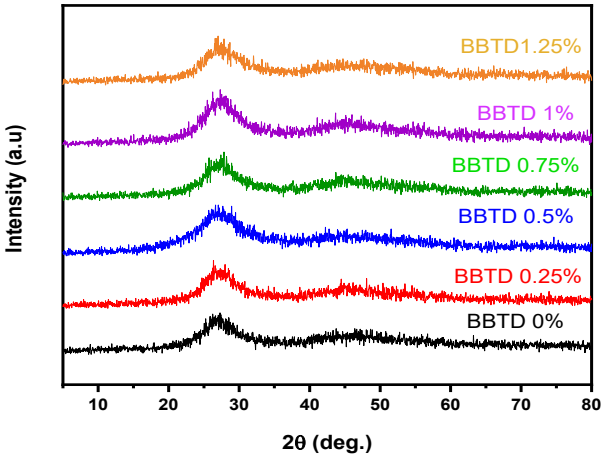

Fig. 1. XRD profiles of as-quenches fabricated glass samples.

Figure 2 shows the room temperature Raman spectrum of the studied glass samples. The analysis was performed using a Renishaw In-Via Reflex micro-Raman spectrometer that use argon ion laser (50 mW) as an excitation source together with a diffraction grating with 2400 lines/mm, an edge filter, and a Peltier-cooled CCD detector. Measurements were performed at room temperature in backscattering geometry with a spectral resolution of 1 cm^{-1}. All the samples showed the spectral peaks related to different functional chemical groups which were consistent with the previous findings [13, 14]. Raman profiles of the samples displayed three distinct wavenumber regions with a broad envelope in the range of 300-452 cm^{-1}, a weak band at 300 cm^{-1} and strong band at 750 cm^{-1} wherein the peak intensity was increased with the increase of dysprosium concentration. The weak band of absorption band was due to the vibration modes of barium oxide [8, 15]. The band at 450 cm^{-1} was associated with the symmetric vibrations of the intra-chain bridging of Te–O–Te [15, 16]. Tagiara [17] also reported the bending vibrations of O-Te-O in TeO_4 tbp units at 450 cm^{-1}. Furthermore, the vibrations modes of both TeO_4 tbp units and Te-O-Te bridges were overlapped around 750 cm^{-1} [13] [18]. The Raman spectra clearly showed an increasing number of [TeO_4] units with the decreasing number of [TeO_3] units. The transformation of [TeO_3] structural units into [TeO_4] units could significantly improve the number of BOs, thus enhancing the glass structural network.

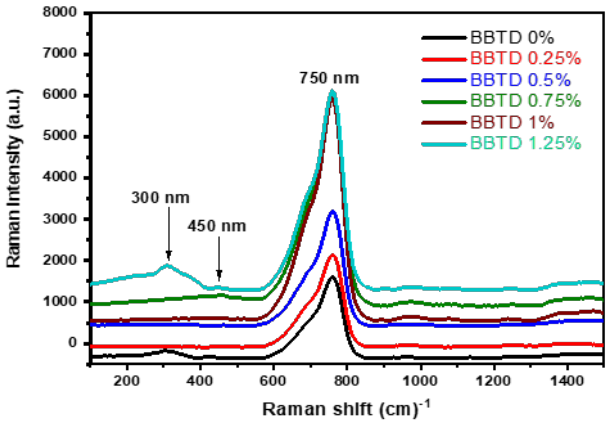

Fig. 2. Raman spectra of fabricated glasses sample.

3.2. UV–Vis absorption spectral analyses of glasses

Figure 3 displays the UV-Vis absorption spectra of the glass samples that were synthesized. As the concentration of Dy^{3+} increased from 0.25 to 1.25 mol%, seven distinct bands were observed at 390, 424, 452, 750, 797, 895, and 1092 nm. These bands corresponded to the... $^6H_{15/2} \rightarrow {}^4F_{7/2}$, $^6H_{15/2} \rightarrow {}^4G_{15/2}$, $^6H_{15/2} \rightarrow {}^4I_{15/2}$, $^6H_{15/2} \rightarrow {}^4F_{9/2}$, $^6H_{15/2} \rightarrow {}^6F_{3/2}$, $^6H_{15/2} \rightarrow {}^6F_{7/2}$, $^6F_{3/2}$, and $^6H_{15/2} \rightarrow {}^6H_{7/2}$+ $^6F_{7/2}$ transitions in Dy^{3+}. The intensity of the absorption peaks were increased with the rise of Dy_2O_3 contents from 0.25 to 1.25 mol%. This observed improvement in the glass absorbance was due to the occupation of Dy^{3+} in the position of B_2O_3. In this study, the UV edge in the optical absorption spectrum was employed to investigate the band gap energies, both direct and indirect, and the electronic band structures of the glass system under examination. The optical absorption coefficient measurement near the fundamental absorption edge served as a standard method to examine optically induced electronic transitions in various materials. This technique allowed for the characterization of the energy levels involved in the absorption process and provided valuable insights into the electronic properties of the material. By analysing the absorption spectrum, it was possible to determine the band gap energy, which is a crucial parameter for understanding the optical and electrical behaviour of the material. Additionally, the measurement of the optical absorption coefficient near the fundamental absorption edge offered information about the nature and type of electronic transitions occurring within the material, such as direct or indirect transitions. Overall, this approach provided a comprehensive understanding of the electronic structure and optical properties of the glass system under investigation. [19].

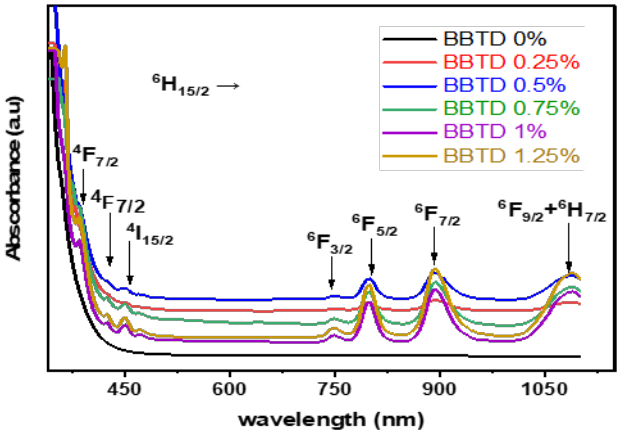

Fig. 3. Optical absorption spectra of glasses.

The fundamental absorption edge (λ cutoff) of the studied glasses showed a shift with the increase of Dy^{3+} contents [20]. The frequency dependent absorption coefficient, $\alpha(v)$ of the glasses at a particular incident photon energy (hv) was calculated from the absorbance A = 2.304/t (with t is the sample thickness equal to 3 mm) [21, 22]. Davis and Mott equation was used to determine the direct and indirect optical band gap energy (E_{opt} in eV) from the generated Tauc plot (Figure 4) [14]. Tauc plots was generated using the expression [23]:

$$\alpha(v) = \frac{A(hv - E_{opt})^r}{hv} \quad (1)$$

where the exponent (r) of this formula differs according to the mechanism of the inter-band transition including direct allowed, direct forbidden, indirect allowed, and indirect forbidden optical transitions [24]. The increase of BOs associated with the increase of Dy^{+3} contents reduced the number of donor centres in the glasses [25], thus widening the optical band gap energies (from 3.155 to 2.1894) at higher doping level of 0.75, 1.0 and 1.25 mol% (Figure 5).

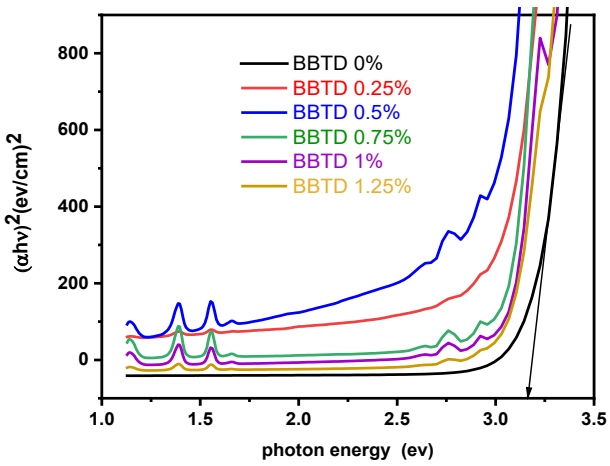

Fig. 4. Tauc plot of the glasses for the evaluation of optical band gap energy.

The glassy nature of the obtained samples was confirmed by calculating the Urbach energy (Eu), indicating their extent of disorders in the matrix [5, 26]. The Urbach energy being associated with valence and conduction bands of the material [27] it can be determined from Eopt using [28]:

$$\alpha(\upsilon) = \beta \exp\left(\frac{h\upsilon}{\Delta E}\right) \tag{2}$$

A plot of ln α against hυ was created to calculate the inverse of the gradients of the linear section. Table 2 provides information on the Urbach energy values of the glass samples. The optical energy band gap exhibited an inverse relationship with the Urbach energy (Figure 5). The values of Eu were decreased and E_{opt} were increase with the increase of Dy_2O_3 content, which was mainly due to the generation of more BOs in the glass network and destruction of NBOs [29]. In short, with the increase of Dy_2O_3 contents the NBO number was reduced, as oxygen anions enhanced the number of TeO_4 units. It is known that the glass network structures with a low Urbach energy tend to have less disorders [30]. In the present glass system, the number of NBOs and BO_3 units was decreased with the raise of Dy^{+3} concentration, causing the network structures more compact [31].A reduction in the Urbach energy can be explained by the fewer defects being created [32].

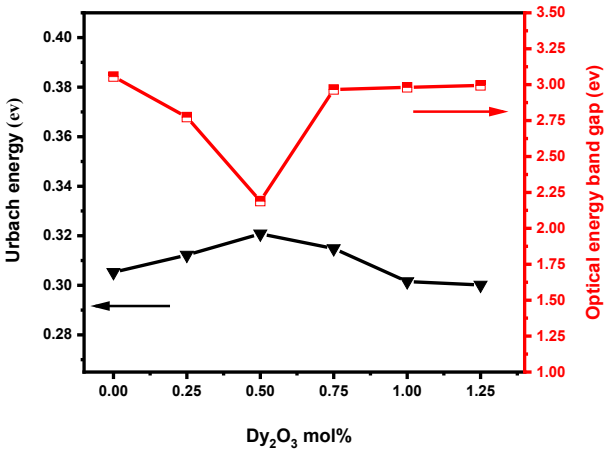

Fig. 5. Dy_2O_3 contents dependent optical band gap and Urbach energy of the glasses.

The refractive indices of the glasses determine how well light can pass through it. Following the Lorenz-Lorentz equation [33], the values of glass refractive indices were evaluated (Table 2):

$$\frac{n^2-1}{n^2+2} = 1 - \sqrt{\frac{E_g}{20}} \tag{3}$$

The refractive indices of the glass system displayed an inverse relation with the values of Eopt. For all the studied glasses, the value of n was about 2.5 (high), indicating their potential applications in photo-cells and optical filters [34]. The values of n for the glasses were ranged from 2.356 to 2.6584 at lower concentration of Dy_2O_3 (0.25 to 0.5 mol%). As shown in Figure 6, the refractive index of the glasses was first increased and then decreased from 2.406 to 2.398 with increase of Dy_2O_3 contents from 0.75 to 1.25 mol% due to a decrease in the electronic polarizability and generation of more BOs [35]. The molar refractivity of the glasses was obtained using the Volf and Lorentz-Lorenz equations in terms of the molar volume (Vm) and n [36]:

$$R_m = \frac{n^2-1}{n^2+2} \times V_m \tag{4}$$

The polarizability of the glasses is an indicator of their ability to react to the applied electric fields. The molar polarizability of the glasses were obtained via [35]:

$$\alpha_m = \frac{3}{4\pi N_A} R_m \tag{5}$$

The relationship between molar polarizability and molar refractive index was utilized to calculate molar electronic polarizability of the glasses using [37]:

$$\alpha_m = \frac{R_m}{2.52} \tag{6}$$

Figure 6 displays the Dy_2O_3 contents dependent variation in the values of n, molar refractive index and molar electronic polarizability of the glasses. The number of NBOs showed a tendency to polarize more than bridging oxygen (BOs). Increasing the concentration of Dy_2O_3 along with reducing the molar refractive index and molar electronic polarizability of the samples demonstrate the formation of bridging oxygen (BOs) resulting in a less polarized sample [37]. The values of the refractive index and electronic polarizability are listed in Table 2.

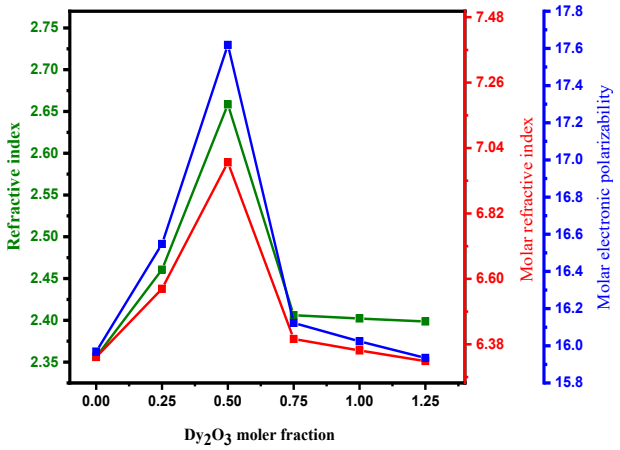

Fig. 6. Dy_2O_3 contents dependent variation in the values of refractive index, molar refractive index and molar electronic polarizability of the glasses.

Fresnel's equation was used to calculate the reflection loss (R_L) at the glass surface [38, 39]. The transmission coefficient (T) was obtained via [39, 40]:

$$R_L = [\frac{n-1}{n+1}]^2 \quad (7)$$

$$T = \frac{2n}{n^2+1} \quad (8)$$

Figure 7 illustrates the Dy^{+3} concentration dependent reflection loss and transmission coefficient of the glasses wherein R_L exhibited an inverse relationship with T (Table 2). A decrease in the value of R_L indicated a decrease of the molar refractivity [41].

Table 2. Some essential optical parameters of the studied glasses. Optical energy band gap, Urbach energy, Refractive index, Molar refractive index, Molar electronic polarizability, Reflection loss & Transmission coefficient.

Dy_2O_3 contents (mol%)	E_{opt} (eV)	ΔE (eV)	n	R_m	α_m	R_L	T
BBTD 0%	3.1559	0.30527	2.35631	6.3371	15.969	0.1633	0.71924
BBTD 0.25%	2.7742	0.31224	2.4607	6.56667	16.548	0.1781	0.69757
BBTD 0.5%	2.1894	0.32081	2.65842	6.99187	17.619	0.2054	0.6590
BBTD 0.75%	2.9665	0.31487	2.40615	6.39807	16.123	0.1704	0.70877
BBTD 1%	2.9811	0.30152	2.40218	6.35905	16.024	0.1698	0.70960
BBTD 1.25%	2.9945	0.30012	2.39856	6.32351	15.935	0.1693	0.71035

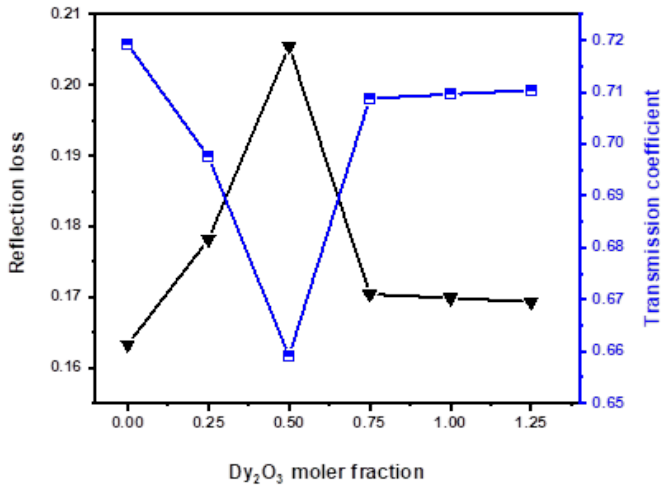

Fig. 7. Dy^{+3} concentration dependent reflection loss and transmission coefficient of the glasses.

It is known that the NBO tends to polarize the glass more than BO. When the molecular refractive index as well as the polarizability (α_m and α_0) with Dy^{+3} concentration was increased, more BO was created [42]. Both values ($\alpha_{o(n)}$ and $\alpha_{02-Eopt}$) were initially increased then dropped at higher concentration of Dy_2O_3 (Figure 8 and Table 3). Higher electronic polarizability of the glasses contradicted to the molar refractivity [34, 35]. The electronic polarizability of the oxygen ions was calculated via [43]:

$$\propto_{o2-E_{opt}} = [\frac{v_m}{2.52}\left(1-\sqrt{\frac{E_{opt}}{20}}\right) - \sum_i \propto_i](N_{O2-})^{-1} \quad (9)$$

The polarizability of the oxide ions was calculated based on the refractive index [9]:

$$\alpha_{o(n)} = [\frac{R_m}{2.52} - \sum \alpha_i](N_{02-})^{-1} \quad (10)$$

where $\sum \alpha i$ and No_2- correspond to the molar cation polarizability and oxide ions number in the glass chemical composition.

In the presence of Dy_2O_3 contents of 0, 0.25, and 0.5 mol% and due to the formation of oxygen molecules that cannot form BO, the free electrons increased the polarizability of the oxide ions [44]. Due to the formation of BOs at higher contents of Dy_2O_3, the oxide iond polarizability was decreased. Since the nuclear charge has less control over the charge distribution, free electrons are more polarizable. The difference between $\alpha_{-o(n)}$ and $\alpha_{o2-Eopt}$ can be interpreted using the David-Mott's theory of non-crystalline conduction wherein the existence of localized states in the band gap play a significant role[42] . This clearly indicates a strong correlation between the structural and spectroscopic properties of the glasses.

According to El-khoshkhany et al. [45] the glass acidity or basicity can be determined by the electron donor power of the oxygen atoms. An acid is a compound that has a low ability to donate electrons and a high chemical resistance. Bases are oxides that donate electrons more readily, but have a lower chemical hardness. Duffy and Ingram reported [46] a relationship between the oxide ions polarizability ($\alpha o2$-) and optical basicity (Λ) via the relation:

$$\Lambda = 1.67(1 - \frac{1}{\alpha_{O2-}}) \quad (11)$$

In glasses, the optical basicity is related to oxygen's electron donor power. High values of Λ indicate ionic bonding, whereas low values of Λ indicate covalent bonding. This allows the type of bonds found in glasses to be calculated. When the polarizability decreases, the optical basicity decreases, resulting in a decrease in refractive index and a rise in optical band gap [47]. The value of optical basicity of the glasses is listed in Table 3. Figure 8 show Dy^{+3} contents dependent optical basicity of the glasses (Figure 8).

The metallization criterion (M) of glasses was calculated using the following equation and the values were in the range of 0.35 and 0.45 [24]:

$$M = 1 - \frac{R_m}{V_M} \quad (12)$$

According to these criteria, a material can be regarded as metallic if Rm/Vm > 1 or non-metallic if Rm/Vm < 1 [48]. For oxide glasses with excellent nonlinear optical characteristics the values of M ranged from 0.30 to 0.45. For the tellurite glass system if the value of M ranged from 0.35 to 0.45 then it is considered as an insulator, while for M values closer to 1 is considered as glass [23, 34]. Saeed et al., [49] reported a value of M less than 1, indicating a much wider valence and conduction band. In the present case, the observed reduction of the M value from 0.39723 - 0.3308 can be ascribed to the decrease of Eopt and the increase of n at lower Dy_2O_3 contents [50]. As shown in Figure 9 and Table 3 with the rise of E_{opt} the values of M were reduction (from 0.5), leading a broader conduction and valence bands [47]. In addition, the values of M for the current glasses were better than other reported glasses, indicating their effectiveness for the non-linear optical applications [34, 51].

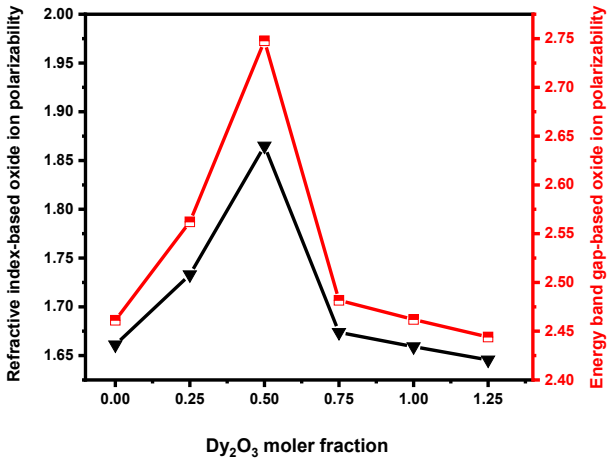

Fig. 8. The refractive index-based polarizability of oxide ions and polarizability based on energy band gap of the glasses.

Based on the glass refractive index and dielectric constant (ε static) were calculated following [52] and [53]. There is a direct relationship between the dielectric function (constant) and energy band gap. We used the formula (13) reported by [9] to calculate the dielectric constant in this study

$$\varepsilon_{static} = n^2 \tag{13}$$

Following the procedure referred in [52], a relationship amid the optical dielectric constant, refractive index, polarization (p), and static dielectric constant was established to determine the optical static dielectric constant:

$$\varepsilon_{opt} = p\frac{dt}{dp} = \varepsilon_{static} - 1 = n^2 - 1 \tag{14}$$

One of the most important properties of dielectric materials is their electrical susceptibility. Measurement of polarizing strength of anamorphous materials can be done using it. Following [54] the electrical susceptibility (χe) was calculated:

$$\chi_e = \frac{n^2-1}{4\pi} \tag{15}$$

The generation of more BO in the glass system led to a decrease in the values of χe [41]. First the values of χe were increased with the increase of Dy_2O_3 contents and then decreased at higher Dy_2O_3 level (Table 3). In addition, the values of ε_{opt} and ε were correspondingly reduced from 4.7704-4.7530 and 5.789580-5.7530 with the raise of Dy_2O_3 contents in the glass system (Figure 10). The values of χ_e were reduced from 0.3798 to 0.3784 with the increase of Dy_2O_3 contents in the glass network due to the decrease of NBOs [21].

Table 3. The refractive index-based polarizability of oxide ions, energy band gap-based polarizability, optical basicity, metallization criterion, dielectric constant, optical dielectric constant, and electrical susceptibility of the glasses.

Dy_2O_3 contents (mol%)	$\propto_{o2-E_{opt}}$	$\alpha_{o(n)}$	Λ	M	ε_{static}	ε_{opt}	χ_e
0	2.461181	1.661035	0.99146	0.39723	5.55222	4.55222	0.3624379
0.25	2.56208	1.732955	1.01819	0.37244	6.055033	5.055033	0.4024708
0.5	2.747728	1.864916	1.06223	0.33086	7.067210	6.067210	0.4830581
0.75	2.481598	1.673762	0.99705	0.38513	5.789580	4.789580	0.3813360
1	2.462040	1.659130	0.9917	0.38608	5.770482	4.770482	0.3798154
1.25	2.444025	1.645602	0.9867	0.38694	5.753076	4.753076	0.3784296

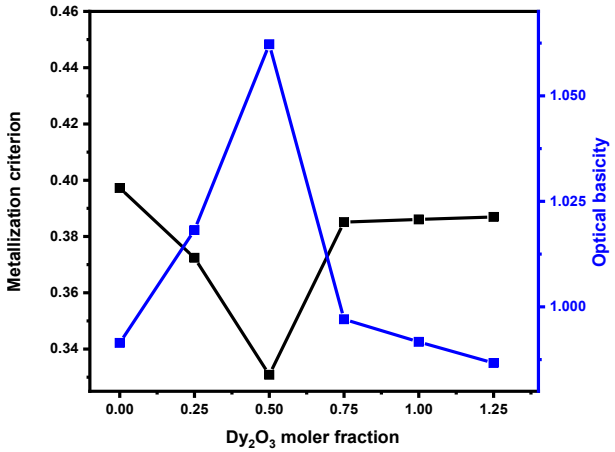

Fig. 9. Optical basicity and metallization criterion of the glasses.

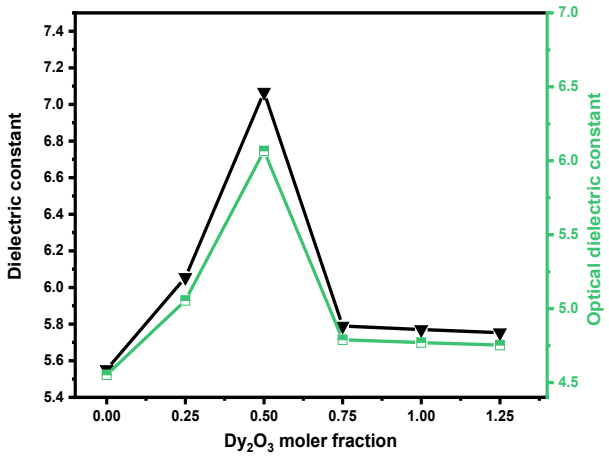

Fig. 10. Dielectric constant, Optical dielectric constant of Dy^{+3} doped BBTD glasses.

3.3. Emission spectral analyses of glasses

Figure 11 displays the room temperature emission spectra of the glasses under excitation wavelength of 400 nm. A Perkin Elmer's LtS55 Luminescence Spectrophotometer was used to measure emission properties in the range of 200 and 1300 nm. A Monk-Gillieson monochromator was used to analyze the excitation and emission energies of the glasses. The intensity of the emission peaks were gradually increased with the increase of Dy^{3+} contents which agreed with the

other findings [55, 56]. The observed 4 prominent luminescence peaks at 474, 485, 564, and 580 nm corresponded to the $^4F_{9/2} \rightarrow {}^6H_{15/2}$, $^4F_{9/2} \rightarrow {}^6H_{15/2}$, $^4F_{9/2} \rightarrow {}^6H_{13/2}$ and $^4F_{9/2} \rightarrow {}^6H_{13/2}$ transitions in Dy^{3+} [57]. The blue transitions (at 474 and 48 5nm) exhibited lower intensity than the yellow transitions (at 564 and 580), indicating the significant role of Dy^{3+} doping in the glass matrix [58] . To explain the observed emission behaviour of the glasses a schematic partial energy level diagram of Dy^{3+} was used (Figure 12). During the excitation at 375 nm, Dy^{3+} was excited from the lower level ($^6H_{15/2}$) to the higher level ($^4F_{9/2}$). There are two prominent emission bands like $^6H_{15/2}$ (blue) and $^6H_{13/2}$ (yellow). Compared with other reported glass matrices, that doped dysprosium ions exhibit good spectroscopic and luminescence properties for yellow lighting applications. As a result of these emissions, especially those in the visible range of light, the composition may be more sensitive and can be used in a variety of applications, including solar cells and sensors [56].

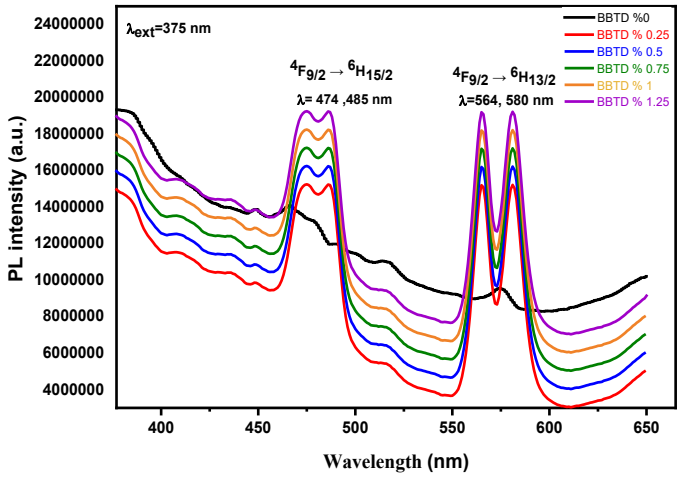

Fig. 11. Emission spectra of glasses under 400 nm excitation.

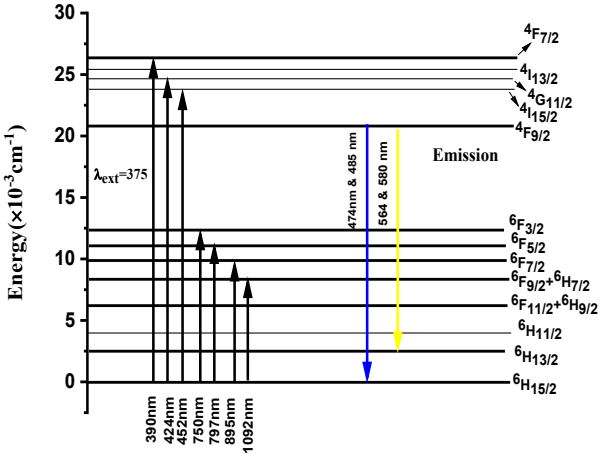

Fig. 12. A schematic energy level diagram of dysprosium ion showing various transitions.

4. Conclusion

Barium-boro-tellurite glasses of composition B_2O_3-BaO-TeO_2 doped with Dy_2O_3 were synthesized using melt-quenching approach and characterized. The structural analyses (XRD and Raman) of the glasses showed appreciable effect of Dy_2O_3 concentration variation on the glass network structures. The absorption and emission spectral analyses of the glasses showed a strong correlation with the structural alteration due to Dy_2O_3 doping wherein more BOs were formed thereby improving the overall physical characteristics of the glasses. At higher Dy_2O_3 doping

contents (0.75, 1, 1.25 mol%), the optical band gap and refractive index was increased. The Urbach energy was first decreased and then gradually increased with the raise of Dy_2O_3 doping. Oxygen anions such as TeO_4 were increased with the raise of Dy_2O_3 contents, causing fewer NBO to form. The values of molar refraction, electronic polarizability and electrical susceptibility of the glass system were decreased with the increase of Dy_2O_3 doping level due to the increase of more BOs. Consequently, the metallization criterion, oxide polarizability, and optical basicity were reduced. The emission spectrum of the glasses displayed 4 intense peaks at 474, 485, 564, and 580 nm. A correlation between the structural and spectroscopic attributes of the glasses was ascertained. It was asserted that the proposed glass composition may be useful for solar cell, solid-state laser and sensor applications.

References

[1] Elkhoshkhany, N., et al., Journal of Non-Crystalline Solids, 2017. 476: p. 15-24; https://doi.org/10.1016/j.jnoncrysol.2017.06.031

[2] Souri, D., Measurement, 2011. 44(4): p. 717-721; https://doi.org/10.1016/j.measurement.2011.01.006

[3] Dahiya, J., et al., Optical Materials, 2022. 134: p. 113162; https://doi.org/10.1016/j.optmat.2022.113162

[4] Farouk, M., et al., Journal of non-crystalline solids, 2013. 371: p. 14-21; https://doi.org/10.1016/j.jnoncrysol.2013.04.001

[5] Halimah, M.K., et al., Results in Physics, 2017. 7: p. 581-589; https://doi.org/10.1016/j.rinp.2017.01.014

[6] Ami Hazlin, M.N., et al., Physica B: Condensed Matter, 2017. 510: p. 38-42; https://doi.org/10.1016/j.physb.2017.01.012

[7] Hazlin, M.A., et al., Physica B: Condensed Matter, 2017. 510: p. 38-42; https://doi.org/10.1016/j.physb.2017.01.012

[8] Halimah, M.K., M.N. Ami Hazlin, F.D. Muhammad, Spectrochimica Acta Part A: Molecular and Biomolecular Spectroscopy, 2018. 195: p. 128-135; https://doi.org/10.1016/j.saa.2017.12.054

[9] Meena, S., B. Bhatia, J. Pure Appl. Ind. Phys., 2016. 6(10): p. 175-183.

[10] Pisarska, J., LOptical materials, 2009. 31(12): p. 1784-1786; https://doi.org/10.1016/j.optmat.2008.11.028

[11] Praveena, R., R. Vijaya, and C. Jayasankar, Spectrochimica Acta Part A: Molecular and Biomolecular Spectroscopy, 2008. 70(3): p. 577-586; https://doi.org/10.1016/j.saa.2007.08.001

[12] Mohd Fudzi, F., et al., Journal of Nanomaterials, 2017. 2017: p. 4150802; https://doi.org/10.1155/2017/4150802

[13] Fares, H., et al., Journal of Non-Crystalline Solids, 2014. 396-397: p. 1-7; https://doi.org/10.1016/j.jnoncrysol.2014.04.012

[14] Fares, H., et al., Journal of Non-Crystalline Solids, 2014. 396: p. 1-7; https://doi.org/10.1016/j.jnoncrysol.2014.04.012

[15] Lalla, E.A., et al., Optical Materials, 2016. 51: p. 35-41; https://doi.org/10.1016/j.optmat.2015.11.010

[16] Nazrin, S., et al., Chalcogenide Letters, 2021. 18(1); https://doi.org/10.15251/CL.2021.181.11

[17] Tagiara, N.S., et al., Journal of Non-Crystalline Solids, 2017. 457: p. 116-125; https://doi.org/10.1016/j.jnoncrysol.2016.11.033

[18] Hill, C. and A. Jha, Journal of non-crystalline solids, 2007. 353(13-15): p. 1372-1376; https://doi.org/10.1016/j.jnoncrysol.2006.10.061

[19] Hogarth, C. and E. Assadzadeh-Kashani, Journal of Materials Science, 1983. 18: p. 1255-1263; https://doi.org/10.1007/BF00551995

[20] Escobar-Alarcón, L., et al., Applied surface science, 2007. 254(1): p. 412-415; https://doi.org/10.1016/j.apsusc.2007.07.052

[21] Algradee, M.A., et al., Optik, 2021. 242: p. 167059; https://doi.org/10.1016/j.ijleo.2021.167059
[22] Mott, N.F. and E.A. Davis, Electronic processes in non-crystalline materials. 2012: Oxford university press.
[23] Hussain, Z., New Journal of Glass and Ceramics, 2021. 11(1): p. 1-33; https://doi.org/10.4236/njgc.2021.111001
[24] Marzouk, S.Y., et al., Optical Materials, 2013. 35(12): p. 2077-2084; https://doi.org/10.1016/j.optmat.2013.05.023
[25] Swapna, G. Upender, M. Prasad, Raman, Journal of Taibah University for Science, 2017. 11(4): p. 583-592; https://doi.org/10.1016/j.jtusci.2016.02.008
[26] Elkhoshkhany, N., M.A. Khatab, M.A. Kabary, Ceramics International, 2018. 44(3): p. 2789-2796; https://doi.org/10.1016/j.ceramint.2017.11.019
[27] Hajer, S., et al., Chalcogenide Letters, 2014. 11(11).
[28] Halimah, M., et al., Mater. Sci. Pol, 2010. 28(1): p. 173-180.
[29] Halimah, M., et al., Results in physics, 2017. 7: p. 581-589; https://doi.org/10.1016/j.rinp.2017.01.014
[30] Obayes, H.K., et al., Journal of Non-Crystalline Solids, 2015. 427: p. 83-90; https://doi.org/10.1016/j.jnoncrysol.2015.07.026
[31] Kolavekar, S.B., N.H. Ayachit, Journal of Materiomics, 2019. 5(3): p. 455-462; https://doi.org/10.1016/j.jmat.2019.01.010
[32] Rammah, Y., et al., Physica B: Condensed Matter, 2020. 583: p. 412055; https://doi.org/10.1016/j.physb.2020.412055
[33] Eevon, C., et al., Results in Physics, 2016. 6: p. 761-766; https://doi.org/10.1016/j.rinp.2016.10.010
[34] Chimalawong, P., et al., Journal of Physics and Chemistry of Solids, 2010. 71(7): p. 965-970; https://doi.org/10.1016/j.jpcs.2010.03.044
[35] Ali, A.A., Y.S. Rammah, M.H. Shaaban, Journal of Non-Crystalline Solids, 2019. 514: p. 52-59; https://doi.org/10.1016/j.jnoncrysol.2019.03.030
[36] Maheshvaran, K., K. Linganna, K. Marimuthu, Journal of Luminescence, 2011. 131(12): p. 2746-2753; https://doi.org/10.1016/j.jlumin.2011.06.047
[37] Umar, S.A., et al., Journal of Non-Crystalline Solids, 2017. 471: p. 101-109; https://doi.org/10.1016/j.jnoncrysol.2017.05.018
[38] Linda, D., et al., Journal of Alloys and Compounds, 2013. 561: p. 151-160; https://doi.org/10.1016/j.jallcom.2013.01.172
[39] Kolavekar, S.B., N.H. Ayachit, Materials Chemistry and Physics, 2021. 257: p. 123796; https://doi.org/10.1016/j.matchemphys.2020.123796
[40] Azlan, M.N., et al., Materials Express, 2015. 5(3): p. 211-218; https://doi.org/10.1166/mex.2015.1236
[41] Dimitrov, V., S. Sakka, Journal of Applied Physics, 1996. 79(3): p. 1736-1740; https://doi.org/10.1063/1.360962
[42] Zhao, X., et al., Physica B: Condensed Matter, 2007. 392(1-2): p. 132-136; https://doi.org/10.1016/j.physb.2006.11.015
[43] Elkhoshkhany, N., et al., Ceramics International, 2014. 40(9): p. 14477-14481; https://doi.org/10.1016/j.ceramint.2014.07.006
[44] Duffy, J.A., Physics and chemistry of glasses, 1989. 30(1): p. 1-4.
[45] Bhatia, B., et al., New Journal of Glass and Ceramics, 2015. 5(03): p. 44; https://doi.org/10.4236/njgc.2015.53006
[46] Umar, S.A., et al., Journal of Non-Crystalline Solids, 2017. 472: p. 31-38; https://doi.org/10.1016/j.jnoncrysol.2017.07.013
[47] Saeed, A., Y. Elbashar, S. El Khameesy, ASilicon, 2018. 10: p. 569-574; https://doi.org/10.1007/s12633-016-9492-y

[48] Amat, A., et al., Electronic Polarizability and Optical Basicity of BaO-B2O3-TeO2 Glass System. 2021; https://doi.org/10.21203/rs.3.rs-1093838/v1

[49] Halimah, M., S. Nazrin, F. Muhammad, Chalcogenide Letters, 2019. 16(8).

[50] Rammah, Y., et al., Journal of Non-Crystalline Solids, 2020. 544: p. 120162; https://doi.org/10.1016/j.jnoncrysol.2020.120162

[51] Bendow, B., et al., Journal of the American Ceramic Society, 1985. 68(4): p. C-92-C-95; https://doi.org/10.1111/j.1151-2916.1985.tb15303.x

[52] Dresselhaus, M.S., Solid state physics part ii optical properties of solids. Lecture Notes (Massachusetts Institute of Technology, Cambridge, MA), 2001. 17: p. 15-16.

[53] Algradee, M.A., et al., Optik, 2021. 242: p. 167059; https://doi.org/10.1016/j.ijleo.2021.167059

[54] Bulus, I., et al., Science World Journal, 2017. 12(4): p. 98-101.

[55] Bagi Aljewaw, O., et al., Applied Sciences, 2020. 10(22): p. 8183; https://doi.org/10.3390/app10228183

[56] Rekha Rani, P., et al., Journal of Alloys and Compounds, 2019. 787: p. 503-518; https://doi.org/10.1016/j.jallcom.2019.02.088

[57] Deopa, N., et al., Optical Materials, 2018. 75: p. 127-134; https://doi.org/10.1016/j.optmat.2017.09.047